MOFBOTS: Metal–Organic-Framework-Based Biomedical Microrobots

Journal Article

Author(s):
Wang, Xiaopu; Chen, Xiang-Zhong; Alcântara, Carlos C.J.; Sevim, Semih; Hoop, Marcus; Terzopoulou, Anastasia; De Marco, Carmela [iD]; Hu, Chengzhi; de Mello, Andrew J.; Falcaro, Paolo; Furukawa, Shuhei; Nelson, Bradley J.; Puigmarti-Luis, Josep; Pané, Salvador

MOFBOTS: Metal–Organic Framework-based Biomedical Microrobots

Xiaopu Wang, Xiang-Zhong Chen, Carlos C.J. Alcântara, Semih Sevim, Marcus Hoop, Anastasia Terzopoulou, Carmela de Marco, Chengzhi Hu, Andrew J. deMello, Paolo Falcaro, Shuhei Furukawa, Bradley J. Nelson, Josep Puigmartí-Luis,* and Salvador Pané

X. Wang, Dr. X. Chen, C. Alcântara, Dr. M. Hoop, A. Terzopoulou, Dr. C. De Marco, Dr. C. Hu, Prof. B. J. Nelson, and Dr. S. Pané
Institute of Robotics and Intelligent Systems, ETH Zurich, Tannenstrasse 3, CH-8092 Zurich, Switzerland
Current address (C. H.): Department of Mechanical and Energy Engineering, Southern University of Science and Technology, No 1088 xueyuan Blvd. Xili, 518055 Shenzhen, China

S. Sevim, Prof. A. J. DeMello, Dr. J. Puigmartí-Luis
Institute for Chemical and Bioengineering, ETH Zurich, Tannenstrasse 3, CH-8092 Zurich, Switzerland
E-mail: josep.puigmarti@chem.ethz.ch

Prof. P. Falcaro
Institute of Physical and Theoretical Chemistry, Graz University of Technology, Stremayrgasse 9, 8010 Graz, Austria

Prof. S. Furukawa
Institute for Integrated Cell-Material Sciences (WPI-iCeMS), Kyoto University, Yoshida, Sakyo-ku, Kyoto 606-8501, Japan

Abstract:

Motile MOFs are potential candidates to serve as small-scale robotic platforms for applications in environmental remediation, targeted drug delivery, or nanosurgery. Here, we successfully fabricate magnetic helical microstructures coated with a kind of zinc-based MOF, zeolitic imidazole framework-8 (ZIF-8), with biocompatibility characteristics and pH-responsive features. Moreover, we show that this highly integrated multifunctional device can swim along pre-designed tracks under the control of weak rotational magnetic fields. The proposed systems can achieve single cell targeting in a cell culture media and a controlled delivery of cargo payloads inside a complex microfluidic channel network. This new approach towards the fabrication of integrated multifunctional systems will open new avenues in soft microrobotics beyond current applications.

Wireless micro and nanorobots are tiny devices that have the ability to swim in different liquid environments powered by either chemical fuels spread in their surroundings, or by means of external energy sources, such as magnetic fields, electric fields, ultrasound, light, or combinations of these.[1] These small-scale devices have been used for many applications, particularly in the biomedical field.[2] With the ability to convey therapeutic agents or cells to difficult-to-reach sites of the human body, micro and nanorobots have the potential to revolutionize many areas of medicine. Progress in this research field is fundamentally linked to advances in materials science and micro and nanomanufacturing.[1d, 3] While many recently developed materials are suitable candidates as components in micro and nanorobotic platforms, their assimilation into a highly integrated multifunctional device has been an ongoing challenge.[1f]

Currently, interest is focused on providing locomotion to soft structures with high porosity and tunable physicochemical properties, such as metal−organic frameworks (MOFs), because of their potential applications as controllable microcarriers.[4] While initial efforts have been made to produce mobile MOF-based small-scale machines,[4a, 5] the locomotion features of most of these systems lack the level of sophistication of current state-of-the-art micro and nanoswimmers. For example, the controlled directionality of chemically propelled MOF crystals has yet to be addressed.[6] In contrast, while magnetically driven MOFs can be guided using an external magnetic field, their locomotion mechanism is mainly limited to magnetic dragging, which requires high magnetic field gradients.[7]

Here, we present a helical MOF-based micromachine that can swim and follow complex trajectories under the control of weak rotational magnetic fields. We focused our research on zeolitic imidazole framework-8 (ZIF-8) due to its excellent biocompatibility and degradation characteristics in relatively mild acidic conditions.[8] We also show that our highly integrated multifunctional micromachine can successfully release drugs to a designated location, where the pH values are around 6, which corresponds to the similar acidic conditions found in tumor

microenvironments.[9] This integrated micromachine is tumor responsive, it enables selectively automated drug delivery and its motion can be precisely controlled, giving it an advantage over previous drug delivery platforms, which have only achieved one of these key features.[10]

In the fabrication process, two-photon polymerization (2PP) stereolithography was used to generate 3D structures on which MOF crystals were grown through a seeded bottom-up synthesis. We fabricated helical swimmers, also known as artificial bacterial flagella (ABF) with 2PP, (**Figure 1**a) and coated them with nickel and then titanium (Figure 1b) to make them magnetic and biocompatible. Next, the sample was treated with O_2 plasma (Figure 1c) to help the growth of polydopamine (PDA) on the ABF surface (Figure 1d). After functionalization with PDA, MOF crystals were grown on the ABF surface (Figure 1e), as heterogeneous nucleation driven by PDA promotes MOF growth.[11] We focused our investigations on the growth of ZIF-8, because of its exceptional thermal and chemical stability in water media and its pH-responsive features.[12] We used different concentrations and reaction times to ensure a complete coating of PDA functionalized ABFs with ZIF-8, called ZIF-8@ABFs from now on (Figure 1f). Figure 1g shows an SEM image of multiple ZIF-8@ABFs.
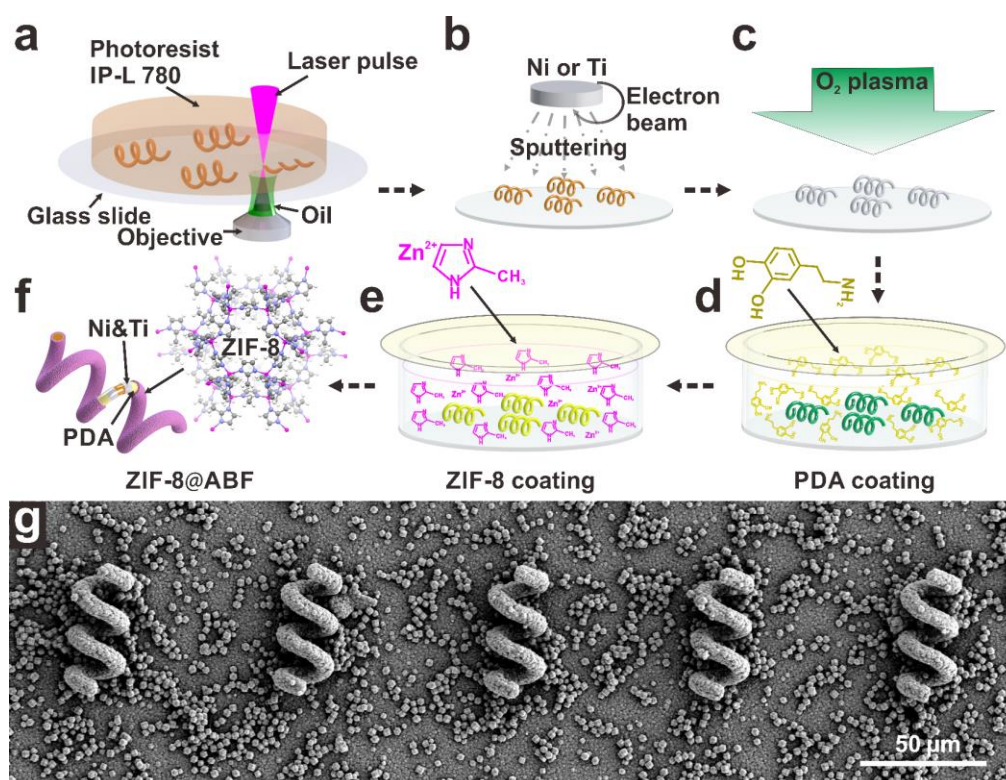
Figure 1. (a-f) Schematic illustration of the component steps involved in the manufacture of ZIF-8@ABF microrobots, detailed explanations can be found in the main text. (g) An SEM image of multiple ZIF-8@ABFs.

As shown in **Figure 2**a, we found that a compact and homogeneous coating with ZIF-8 was achieved by immersing PDA functionalized ABFs in a methanolic solution of $Zn(NO_3)_2$ (25 mM) and 2-methylimidazole (50 mM) for a period of 24 hours. Comparison of ZIF-8 fabricated with different reactant concentrations and reacting times is shown in the supporting information and **Figure S1.** As clearly observed by scanning electron microscopy (SEM), maintaining the same concentrations of reactant but with a reduced reaction time of 2 hours resulted in an undesirable partial coating of the ABF surface (Figure S1). Additionally, under this condition, the synthesized ZIF-8 crystals were not uniform in size, varying between 150 and 450 nm. Conversely, increasing reactant concentrations (i.e. $Zn(NO_3)_2$ 50 mM and 2-methylimidazole 100 mM) while maintaining a reaction time of 24 hours, rendered ZIF-8@ABFs with rough surfaces unsuitable for smooth maneuvering of the composite structures in solution (Figure S1a-VI); this could be caused by an overgrowth of ZIF-8 on ABFs. A decrease in reactant concentrations (i.e. $Zn(NO_3)_2$ 10 mM and 2-methylimidazole 20 mM) resulted in a considerable number of pristine (unmodified) ABF structures, and these conditions were not considered further in our investigation (see Supporting Information and **Figure S2** for further details). Note that in all these experiments, the ratio of zinc nitrate over 2-methylimidazole concentrations was kept constant at a value of 0.5.

After the ZIF-8 coating optimization, ZIF-8@ABFs were characterized using energy dispersive X-ray analysis (EDS) and X-ray diffraction (XRD) studies, to unambiguously confirm the elemental composition and crystalline nature of the MOF structure. EDS analysis with SEM revealed the presence of Zn, N and C throughout the ZIF-8@ABF structures, indicating their compact and homogeneous coating with ZIF-8 crystals (Figure 2b). In addition,

the XRD plot obtained from the powder of the ZIF-8 coating was almost identical to the pattern reported in the literature for ZIF-8 crystals (see Figure S2).[13] These results confirm the sodalite crystalline nature of the ZIF-8 coating on PDA functionalized ABFs.

The swimming behavior of ZIF-8@ABF structures was investigated in water by applying an alternative rotational magnetic field (generated by Helmholtz coils) to a suspension of ZIF-8@ABFs. The relationship between the forward speed of ZIF-8@ABFs and the rotating frequency of the magnetic field at 4 mT is shown in Figure 2c. Three different swimming conditions were clearly identified: (i) wobbling motion below 10 Hz, (ii) corkscrew motion between 10 and 40 Hz, and (iii) step-out condition above 40 Hz. Generally, by increasing the frequency of the rotating magnetic field, the propulsion speed of the helical swimmer increases until the step-out frequency is reached. Note that the step-out frequency is the maximum frequency by which a magnetic swimmer can rotate synchronously with the applied magnetic field. Above this frequency the magnetic body rotates asynchronously. In other words, the swimmer cannot follow the rotating magnetic field, and consequently its propulsion speed decreases as the frequency increases. By changing the direction and the rotating frequency of the magnetic field, the ZIF-8@ABF can be navigated along a user-designed path. Figure 2d shows the trajectory of a ZIF-8@ABF tracking a pre-designed pattern "m". **Video S1** reports the trajectory of a ZIF-8@ABF writing the letters "mof". This controlled motion can also be extended to a third dimension as shown in **Video S2**. These results demonstrate that the mobility and location of ZIF-8@ABFs can be precisely remotely controlled.
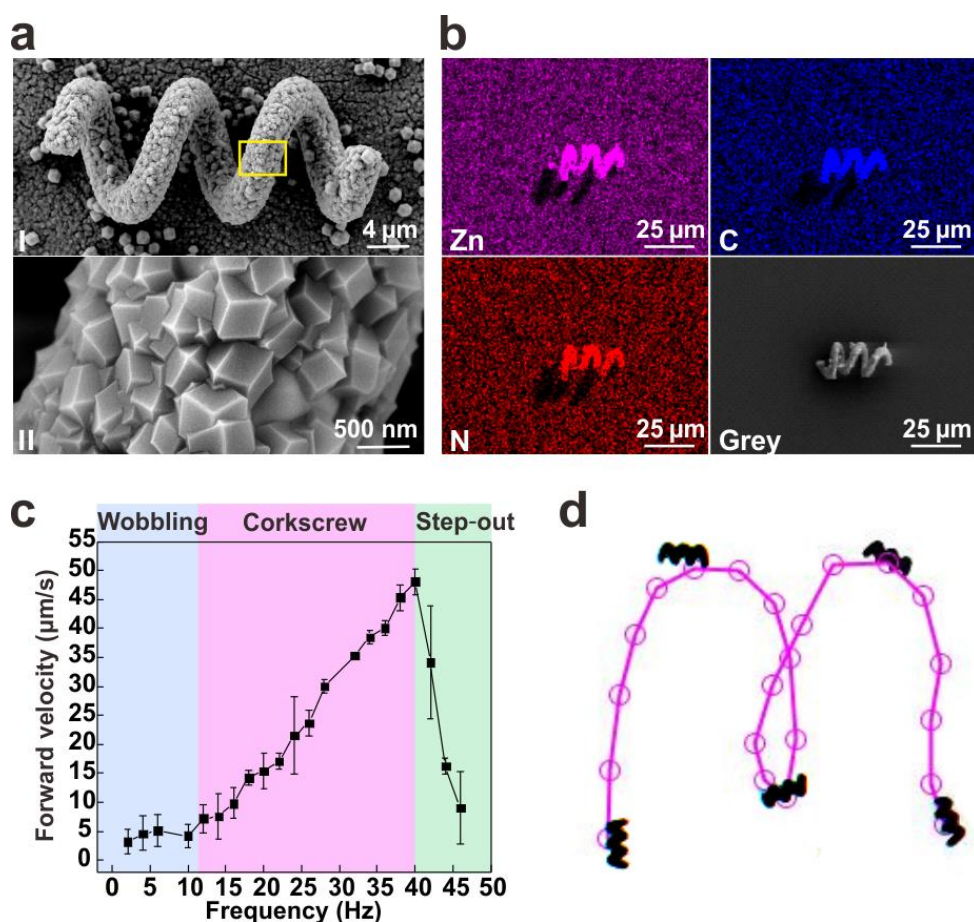
Figure 2. (a) (i) SEM images of ZIF-8@ABFs fabricated after 24 hours in a methanolic solution of $Zn(NO_3)_2$ (25 mM) and 2-methylimidazole (50 mM) & (ii) An enlarged SEM image of the area marked by the yellow box in panel (i). (b) SEM-EDX images of a ZIF-8@ABF structure. (c) Variation of the forward velocity as a function of frequency for ZIF-8@ABFs when applying a rotational magnetic field of 4 mT. Each point corresponds to the average speed of three ZIF-8@ABF microrobots (n=3). (d) Trajectory of a ZIF-8@ABF microrobot following a pre-designed track.

SEM investigations revealed that the integrity of ZIF-8@ABFs was maintained even when the structures were kept for 24 hours in a phosphate buffer solution (PBS) at pH 7.4 (**Figure 3**a). However, as shown in Figure 3a, ZIF-8 crystals on ZIF-8@ABFs were significantly degraded after being exposed to a slightly acidic PBS solution (pH 6.0) for a period of 12 hours. It has been reported that mildly acidic conditions can prompt the degradation of

ZIF-8 crystals,[8] which makes this material ideal for drug delivery applications in cancer therapy, as cancer cells are typically surrounded by a different environment than that of normal cells. Note that changes or gradients in pH in body fluids have been a source of inspiration for the development of several pH-responsive micro- and nanoswimmers[14]. The extracellular medium in cancerous tissues has been shown to exhibit a slightly acidic pH, with values ranging from 5 to 6.[9] Accordingly, the pH dependent stability of ZIF-8 on ZIF-8@ABFs provides an unprecedented system (the mobile 3D MOF structure) that behaves as a pH-responsive microrobot for targeted drug delivery applications.

To confirm the potential of ZIF-8@ABFs as drug carrier microrobots, we loaded fluorescent Rhodamine B (RhB) as a drug model compound to the ZIF-8 crystals of ZIF-8@ABFs, hereafter referred to as RhB@ZIF-8@ABFs. The encapsulation of RhB in ZIF-8 was carried out following a one-pot protocol, as described in the literature, but with some minor modifications.[8c] RhB@ZIF-8@ABFs were fabricated by immersing PDA functionalized ABFs in a methanolic solution of $Zn(NO_3)_2$ (25 mM), 2-methylimidazole (50 mM) and RhB (1 mM) for 24 hours. Figure 3b shows the bright field and fluorescence images of a ZIF-8@ABF, an RhB@ZIF-8@ABF, and a control sample. The control sample corresponds to an ABF incubated with a methanolic solution of RhB (1 mM) for 24 hours in the absence of ZIF-8 precursors. From the micrographs shown in Figure 3b and 3c, we can see that RhB is only loaded in RhB@ZIF-8@ABFs. Moreover, to demonstrate the targeted drug delivery capabilities of motile RhB@ZIF-8@ABFs in biologically relevant media, we show that these devices can supply therapeutic payloads to a target region within a cell culture. Figure 3d shows the fluorescent images of an RhB@ZIF-8@ABF which was maneuvered to a specific target cell localized on the surface of a Petri dish (see also **Video S3** in the Supporting Information). Note that the RhB@ZIF-8@ABF was navigated along a pre-designed customized trajectory towards a single cell, without touching any adjacent cells.
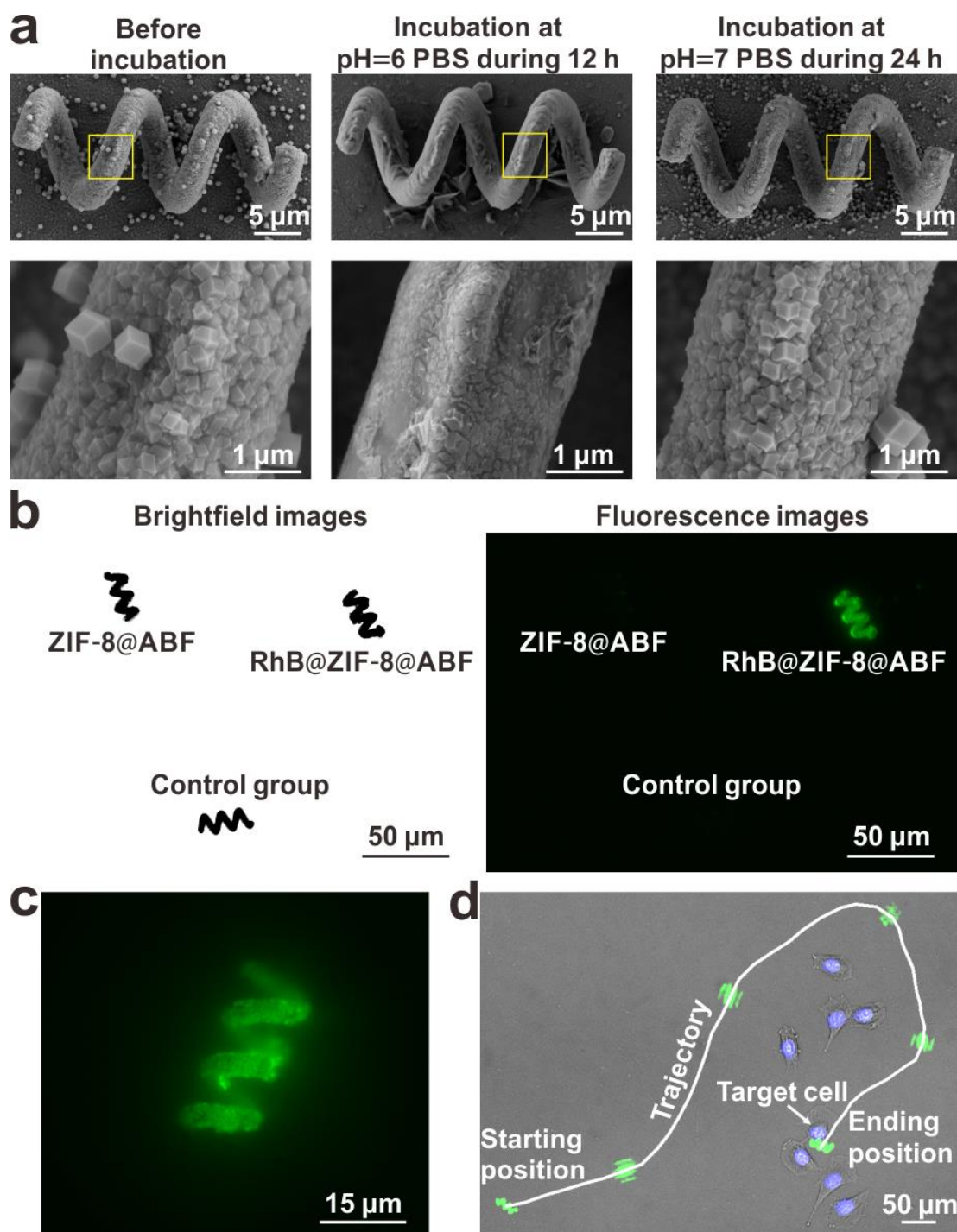
Figure 3. (a) From left to right, SEM images of ZIF-8@ABF before incubation, after 12 hours incubation at pH 6.0, and after 24 hours incubation at pH 7.0. The series of SEM images in the bottom row are magnifications of the SEM images presented in the top row. (b) Bright field and fluorescence images of a ZIF-8@ABF, an RhB@ZIF-8@ABF, and a control sample (ABF). (c) Magnified fluorescence image of an RhB@ZIF-8@ABF. (d) Micrograph showing the

movement of an RhB@ZIF-8@ABF structure along a complex trajectory, targeting a single cell.

Under acidic buffer conditions (i.e. PBS at pH 6.0), RhB was clearly transferred from RhB@ZIF-8@ABFs to breast cancer cells (MDA-MB231) located on the surface of a Petri dish. **Figure 4** shows the brightfield and fluorescence images of breast cancer cells after being incubated for 3 hours with RhB@ZIF-8@ABFs at pH 7.4 and pH 6.0. The data confirms that when RhB@ZIF-8@ABFs are navigated through an acidic environment, such as the extracellular medium of cancer tissues, the cargo loaded in ZIF-8@ABFs can be efficiently transferred to cells. The same swimmers navigated through a pH 7.4 environment remain intact, as confirmed by a lack of cellular emission throughout the field of view. In these experiments, breast cancer cell nuclei were stained with Hoechst 33342 to facilitate visualization of cell positions.
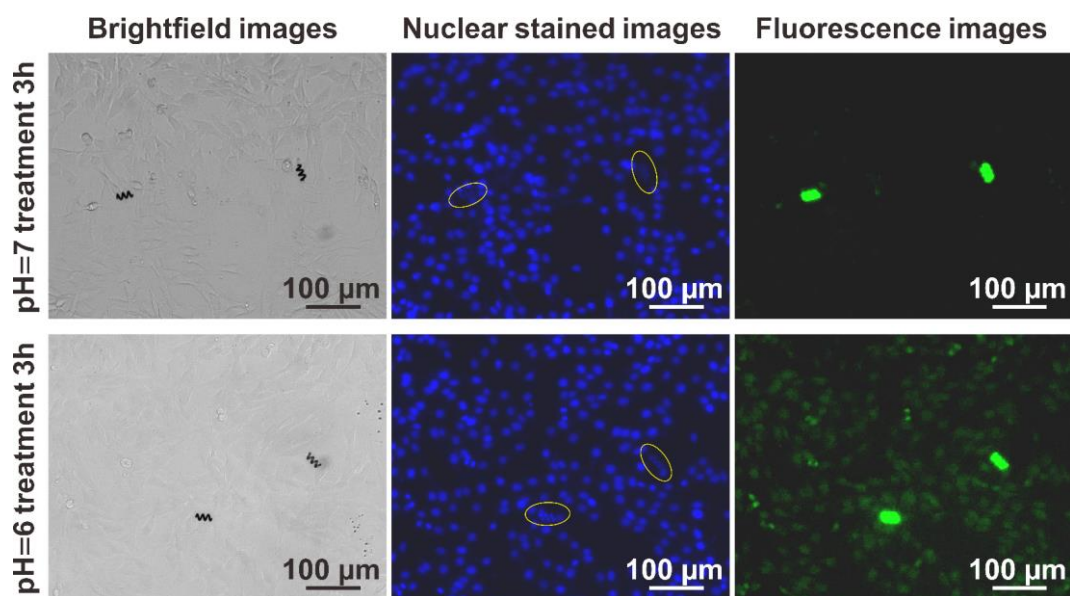

Figure 4. *In vitro* model drug release of RhB@ZIF-8@ABF in PBS (pH 7.4) and PBS (pH 6.0) to fixed breast cancer cells (MDA-MB231)

The controlled motion and drug delivery capabilities of these highly integrated multifunctional systems are further demonstrated within a complex microfluidic system incorporating pneumatic valves (**Figure 5**). This pneumatic microfluidic configuration allows the controllable generation of two distinct microenvironments at pH 5.0 and 7.4 via pneumatic actuation (Figure 5b). Four RhB@ZIF-8@ABFs were introduced at position 1 (P1) of the microfluidic device where the pH is 7.4. The ABFs were then maneuvered towards P4 trapping two ABFs at P4 (pH 5.0) and two ABFs at P2 (pH 7.4). This controlled positioning of the microrobots was achieved via pneumatic actuation of the integrated valves. As illustrated in Figure 5d, the RhB@ZIF-8@ABFs kept in P2 remain fluorescent, while the RhB@ZIF-8@ABFs located in P4 and P5 lose the fluorescence emission. This indicates that ZIF-8 degrades within a low pH environment, accompanied by cargo (RhB) discharge. Accordingly, this model experiment demonstrates that ZIF-8@ABFs are able to dispense drug-like molecules in a selective and controllable manner.
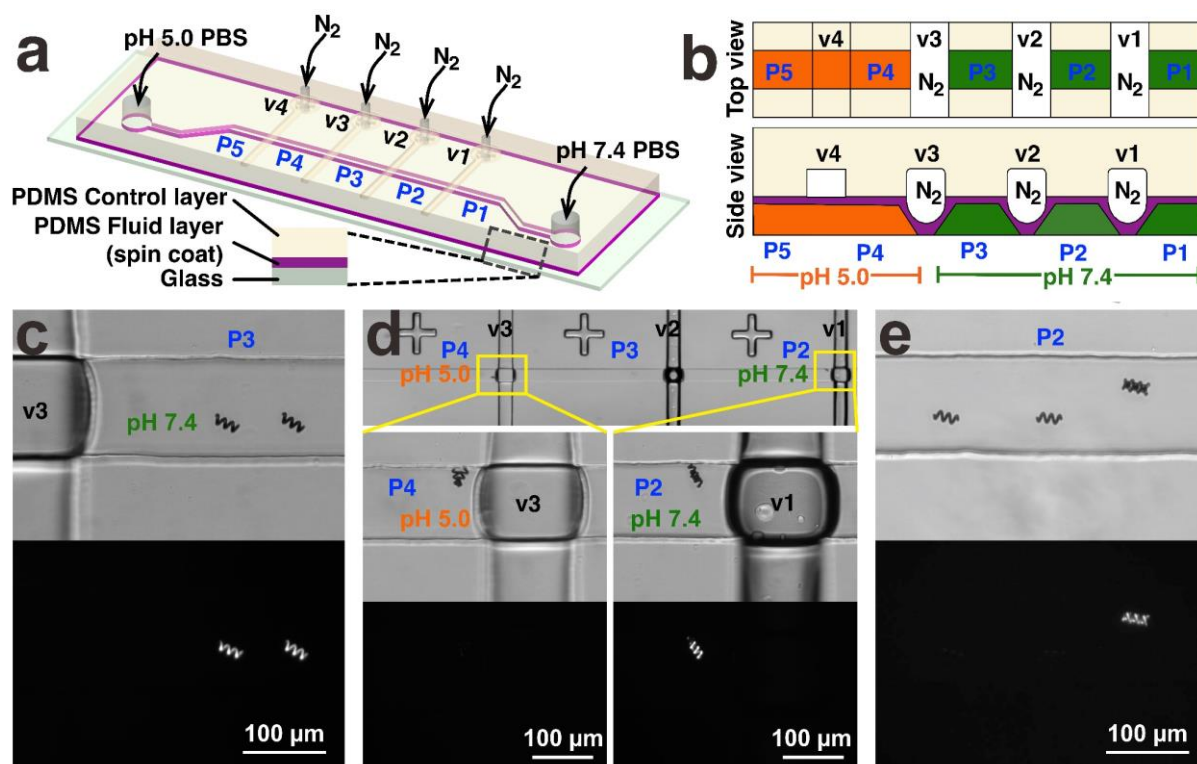
Figure 5. (a) Schematic illustration of the microfluidic device used to demonstrate regioselective delivery of cargo. (b) Side view of the microfluidic device, highlighting the pneumatic actuation of integrated valves. (c-e) Series of brightfield and fluorescence micrographs showing the control manipulation of RhB@ZIF-8@ABFs from P2 to P5 and back.

In summary, we successfully developed an MOF-based ABF. These ABFs can be successfully maneuvered and controlled by magnetic microhelices with a corkscrew locomotion mechanism using only weak external magnetic fields. The MOF-based swimmers consist of a magnetically coated 3D printed helical framework, whose surface is coated with a highly biocompatible and pH-responsive Zn-based MOF (ZIF-8) surface coating. The thickness and compactness of the ZIF-8 coatings on the surface of such helical structures can be tailored by the variation of synthetic conditions (reactants concentration and reaction time). To illustrate the potential of the proposed MOF-based microrobots, we have shown that these swimmers can act as pH-responsive targeted drug delivery platforms, able to carry and release drugs in biologically relevant environments similar to those encountered in the extracellular media of a tumor. We have also demonstrated that the proposed MOF-based microrobots can follow complex trajectories within microfluidic channels to deliver drugs in a regioselective manner.

Experimental Section

Fabrication of ZIF-8@ABFs: The ABFs were fabricated using a 3D Direct Laser lithography (Nanoscribe GmbH). Briefly, photoresist IPL-780 (negative-tone photoresist) was spincoated on a glass substrate. The helical structure was designed with solid works and loaded in the Nanoscribe software. During the two-photon lithography process, the laser power used was 13 mW, and the scan speed was 50 mm/s. Finally, the array of helical structures were developed in IPA for 10 min, and then dried with a nitrogen gun. Based on previous investigations,[15] we chose as a prototypical swimmer a helix with three turns, a helical

diameter of around 10 µm, a filament diameter of approximately 3 µm, and a helical angle around 70°. This design providesd good swimming performance at low magnitude rotating magnetic fields. Additionally, our swimmers exhibited a corkscrew regime at relatively low frequencies (10 Hz). The framework was coated first with nickel (90 nm) and then titanium (9 nm) successively with an electron beam evaporator (Plassys-II MEB550SL). A homogeneous coating was achieved by applying a tilt of 15° and a rotating speed of 20 rpm at the sample stage. The coated framework was then exposed to a O_2 plasma for 90 seconds to clean and oxidize the surface. After construction, the oxidized ABFs were treated with dopamine hydrochloride (2.5 mg/ml) in tris hydroxymethyl aminomethane (10 mM) for 24 hours to grow a polydopamine (PDA) layer on the ABF surface. Two solutions of zinc nitrate hexahydrate (20 mM / 50 mM / 100 mM) and 2-methylimidazole (40 mM / 100 mM / 200 mM) were then prepared in methanol and an equal amount of each solution was mixed and stirred for 1 minute at 500 rpm. PDA-coated ABFs were immersed into the resulting mixture for a specific period of time (2 or 24 hours). Finally, the modified ABFs were washed with methanol and dried with nitrogen.

Characterization of ZIF-8 coatings: SEM images were taken to characterize the surface morphology of ZIF-8@ABFs. In addition, an EDX analysis was performed to confirm the presence of Zn, N and C elements in ZIF-8 crystals. The XRD measurements were obtained from ZIF-8 crystals grown on a polydopamine deposited silicon wafer. For the ZIF-8@ABF synthesis, prior to the polydopamine treatment, the silicon wafer was coated with IPL-780 (polymerized by exposure to a LOT-Oriel 500W Hg UV-Source for 10 minutes), nickel (90 nm) and titanium (9 nm).

ZIF-8@ABF locomotion: The swimming behavior of ZIF-8@ABFs was investigated using an electromagnetic control system consisting of three pairs of Helmholtz coils to generate a rotational magnetic field. A ZIF-8@ABF sample was immersed in deionized water in a sample holder with a piece of clean silicon wafer. The sample holder was then placed at the

13

center of the Helmholtz setup to ensure a uniform magnetic field. A microprobe (T-4-22, GGB Industries, INC., US) was then used to release the ZIF-8@ABF and transport it onto the silicon wafer. A rotational magnetic field of 4 mT was applied to manipulate the ZIF-8@ABF. Variations in the direction and the rotating frequency of the magnetic field were used to maneuver ZIF-8@ABF along pre-defined trajectories.

Stability of ZIF-8@ABF as a function of pH: PBS pH=7.4 (1X) was purchased from Thermo Fisher Scientific. The acidic PBS solution was obtained by adjusting the pH value of PBS from 7.4 to 6.0 using phosphoric acid. The PBS pH 6.0 and pH 5.0 solutions were used below was also obtained using this method. SEM images were acquired after incubating ZIF-8@ABFs at pH 6.0 and pH 7.4 for a given time period.

Fabrication of RhB@ZIF-8@ABF: The fabrication of the ABFs was explained above. RhB was incorporated into the medium used to grow ZIF-8 crystals. RhB (5 mg) was dissolved in a methanol solution containing zinc nitrate hexahydrate (5 ml, 50 mM). A solution of 2-methylimidazole (5 ml, 100 mM) in methanol was then added in drops, and the mixture was stirred at 500 rpm for 1 minute. The PDA treated ABFs were then immersed in the resulting mixture and left to stand for 24 hours. Finally, the samples were washed with methanol and then dried with a nitrogen gun.

Drug delivery within cell culture: 3T3 cells were fixed in a Petri dish using 4% paraformaldehyde in PBS (pH 7.4) and washed with PBS (pH 7.4). The cell nuclei were stained using Hoechst 33342 (Thermo Fisher Scientific), and all cells were kept in PBS at pH 7.4 prior to experimentation. An RhB@ZIF-8@ABF was transferred to the Petri dish using a microprobe (T-4-22, GGB Industries, INC., U.S.). A customized magnetic actuation system (MFG-100-I, MagnetbotiX AG, Switzerland) was used to generate rotational magnetic fields to manipulate the RhB@ZIF-8@ABF to a target region in the cell culture, following a predefined trajectory. Videos and images were taken with a fluorescence inverted optical microscope (Olympus IX-81, Olympus Optical co. Ltd., Japan).

Drug release experiments: Breast cancer cells (MDA-MB231) were fixed in a Petri dish using 4% paraformaldehyde in PBS (pH 7.4) and washed with PBS (pH 7.4). Cell nuclei were stained using Hoechst 33342 (Thermo Fisher Scientific), and all cells were kept in PBS at pH 7.4 prior to experimentation. Two different solutions for cargo release were assessed, PBS pH 6.0 and PBS pH 7.4. After incubating the RhB@ZIF-8@ABF for 3 hours, brightfield and fluorescence images were taken. A blue filter was used to extract fluorescence signals from cell nuclei and RhB, while a green filter was used to extract the fluorescence signal from RhB only.

Microfluidic device fabrication: Double layer, polydimethylsiloxane (PDMS) microfluidic devices were fabricated on silicon wafers (Okmetic, Finland) using conventional soft lithography techniques.[16] The top (control) layer was fabricated using replica molding.[17] First, a mixture of PDMS elastomer and curing agent (Sylgard 184, Dow Corning, Midland, USA) was prepared at a ratio of 5:1 w/w. This mixture was then put under vacuum for 30 minutes to remove trapped gases. The PDMS mixture was then poured on top of the silicon wafer containing the features for the "control layer" and the entire assembly cured at 70ºC for 30 minutes. To make the bottom (fluidic) layer, a degassed mixture of PDMS and curing agent (20:1 in weight) was spin-coated on the fluidic master mold in two consecutive steps (first 500 rpm for 10 seconds, and then 1200 rpm for 50 seconds). After spinning, the "fluidic" master mold was cured at 70ºC for a period of 15 minutes. The control layer was diced using a razor blade, and holes were formed using a Gauge 22 puncher (Technical Innovations Inc., Texas). The control layer was then assembled on top of the cured fluidic layer in the "fluidic" master mold. The two layers were placed in an oven at 70ºC overnight to ensure complete thermal bonding. Following this, the two bonded layers were removed from the "fluidic" master mold, diced with a razor blade, and 1.5 mm holes were formed using a biopsy punch (Miltex GmbH, Rietheim-Weilheim, Germany) in the fluidic layer. Finally, the double layer PDMS devices were bonded to a glass coverslip (24 mm x 60 mm, Menzel Glasbearbeitungswerk GmbH & Co. KG, Germany) using oxygen plasma activation.

15

Loading of RhB@ZIF-8@ABFs and preparation of the microfluidic environment: The microfluidic device was designed with five regions that can be separated by pneumatic actuation of the integrated valves. Each valve consists of a thin PDMS membrane that can be deflected towards the glass substrate when nitrogen is pumped through the top (control) microfluidic layer. In the experiment, RhB@ZIF-8@ABFs were dispensed inside the microfluidic device (P1) through the inlet near P1. Note that valve 1 (V1) was kept closed during the injection of the microrobots to prevent access to the microchamber P2. The RhB@ZIF-8@ABFs were dispensed with ethanol which evaporated after a few hours. A PBS solution (pH 7.4) was introduced in P1, when V1 and V2 were open and V3 was closed. At the same time, a PBS solution (pH 5.0) was injected through the inlet near P5, while V4 was open and V3 was closed. In this way, two well-defined microenvironments at different pH were generated.

Supporting Information
Supporting Information is available from the Wiley Online Library or from the author.

Received: ((will be filled in by the editorial staff))
Revised: ((will be filled in by the editorial staff))
Published online: ((will be filled in by the editorial staff))

References

[1]   a) B. J. Nelson, I. K. Kaliakatsos, J. J. Abbott, Annual review of biomedical engineering 2010, 12, 55; b) J. Wang, W. Gao, ACS nano 2012, 6, 5745; c) X. Wang, C. Hu, L. Schurz, C. De Marco, X. Chen, S. Pané, B. J. Nelson, ACS nano 2018, 12, 6210; d) X. Wang, X. H. Qin,

C. Hu, A. Terzopoulou, X. Z. Chen, T. Y. Huang, K. Maniura‐Weber, S. Pané, B. J. Nelson, Advanced Functional Materials 2018, 28, 1804107; e) D. Ahmed, T. Baasch, B. Jang, S. Pane, J. r. Dual, B. J. Nelson, Nano letters 2016, 16, 4968; f) X.-Z. Chen, N. Shamsudhin, M. Hoop, R. Pieters, E. Siringil, M. S. Sakar, B. J. Nelson, S. Pané, Materials Horizons 2016, 3, 113; g) D. Ahmed, C. Dillinger, A. Hong, B. J. Nelson, Advanced Materials Technologies 2017, 2, 1700050; h) J. Li, B. E.-F. de Ávila, W. Gao, L. Zhang, J. Wang, Sci. Robot. 2017, 2; i) S. C. Lenaghan, Y. Wang, N. Xi, T. Fukuda, T. Tarn, W. R. Hamel, M. Zhang, IEEE Trans Biomed Eng 2013, 60, 667; j) H. M. Li, J. D. Tan, M. J. Zhang, Ieee Transactions on Automation Science and Engineering 2009, 6, 220; k) C. Bi, M. Guix, B. V. Johnson, W. Jing, D. J. Cappelleri, Micromachines (Basel) 2018, 9; l) L. O. Mair, S. Chowdhury, G. A. Paredes-Juarez, M. Guix, C. Bi, B. Johnson, B. W. English, S. Jafari, J. Baker-McKee, J. Watson-Daniels, O. Hale, P. Stepanov, D. Sun, Z. Baker, C. Ropp, S. B. Raval, D. R. Arifin, J. W. M. Bulte, I. N. Weinberg, B. A. Evans, D. J. Cappelleri, Micromachines (Basel) 2019, 10; m) W. Hu, K. S. Ishii, Q. Fan, A. T. Ohta, Lab Chip 2012, 12, 3821.

[2]   a) G. Chatzipirpiridis, O. Ergeneman, J. Pokki, F. Ullrich, S. Fusco, J. A. Ortega, K. M. Sivaraman, B. J. Nelson, S. Pané, Advanced healthcare materials 2015, 4, 209; b) F. Qiu, S. Fujita, R. Mhanna, L. Zhang, B. R. Simona, B. J. Nelson, Advanced Functional Materials 2015, 25, 1666; c) M. Sitti, H. Ceylan, W. Hu, J. Giltinan, M. Turan, S. Yim, E. Diller, Proceedings of the IEEE 2015, 103, 205.

[3]   H.-W. Huang, M. S. Sakar, A. J. Petruska, S. Pané, B. J. Nelson, Nature communications 2016, 7, 12263.

[4]   a) Y. Ikezoe, G. Washino, T. Uemura, S. Kitagawa, H. Matsui, Nature materials 2012, 11, 1081; b) B. Khezri, M. Pumera, Adv Mater 2019, e1806530.

[5]   A. Ayala, C. Carbonell, I. Imaz, D. Maspoch, Chemical Communications 2016, 52, 5096.

[6]   J. Li, X. Yu, M. Xu, W. Liu, E. Sandraz, H. Lan, J. Wang, S. M. Cohen, Journal of the American Chemical Society 2017, 139, 611.

[7]   a) S. K. Elsaidi, M. A. Sinnwell, D. Banerjee, A. Devaraj, R. K. Kukkadapu, T. C. Droubay, Z. Nie, L. Kovarik, M. Vijayakumar, S. Manandhar, Nano letters 2017, 17, 6968; b) G. Lu, S. Li, Z. Guo, O. K. Farha, B. G. Hauser, X. Qi, Y. Wang, X. Wang, S. Han, X. Liu, Nature chemistry 2012, 4, 310; c) P. Falcaro, F. Normandin, M. Takahashi, P. Scopece, H. Amenitsch, S. Costacurta, C. M. Doherty, J. S. Laird, M. D. Lay, F. Lisi, Advanced materials 2011, 23, 3901; d) P. Falcaro, F. Lapierre, B. Marmiroli, M. Styles, Y. Zhu, M. Takahashi, A. J. Hill, C. M. Doherty, Journal of Materials Chemistry C 2013, 1, 42.

[8]   a) C. Y. Sun, C. Qin, X. L. Wang, G. S. Yang, K. Z. Shao, Y. Q. Lan, Z. M. Su, P. Huang, C. G. Wang, E. B. Wang, Dalton T 2012, 41, 6906; b) H. Ren, L. Zhang, J. An, T. Wang, L. Li, X. Si, L. He, X. Wu, C. Wang, Z. Su, Chemical Communications 2014, 50, 1000; c) H. Q. Zheng, Y. N. Zhang, L. F. Liu, W. Wan, P. Guo, A. M. Nystrom, X. D. Zou, Journal of the American Chemical Society 2016, 138, 962.

[9]   Y. Wang, K. Zhou, G. Huang, C. Hensley, X. Huang, X. Ma, T. Zhao, B. D. Sumer, R. J. DeBerardinis, J. Gao, Nature materials 2014, 13, 204.

[10]   a) R. Mhanna, F. Qiu, L. Zhang, Y. Ding, K. Sugihara, M. Zenobi‐Wong, B. J. Nelson, Small 2014, 10, 1953; b) W. Cai, J. Wang, C. Chu, W. Chen, C. Wu, G. Liu, Advanced Science 2019; c) P. Erkoc, I. C. Yasa, H. Ceylan, O. Yasa, Y. Alapan, M. Sitti, Advanced Therapeutics 2019, 2, 1800064.

[11]   a) Q. Ye, F. Zhou, W. Liu, Chemical Society Reviews 2011, 40, 4244; b) Q. Liu, N. Wang, J. Caro, A. Huang, Journal of the American Chemical Society 2013, 135, 17679; c) J. Zhou, P. Wang, C. Wang, Y. T. Goh, Z. Fang, P. B. Messersmith, H. Duan, ACS Nano 2015, 9, 6951.

[12]   A. J. Howarth, Y. Liu, P. Li, Z. Li, T. C. Wang, J. T. Hupp, O. K. Farha, Nature Reviews Materials 2016, 1, 15018.

[13]   D. Fairen-Jimenez, S. Moggach, M. Wharmby, P. Wright, S. Parsons, T. Duren, Journal of the American Chemical Society 2011, 133, 8900.
[14]   a) S. Fusco, G. Chatzipirpiridis, K. M. Sivaraman, O. Ergeneman, B. J. Nelson, S. Pane, Adv Healthc Mater 2013, 2, 1037; b) H. Li, G. Go, S. Y. Ko, J. O. Park, S. Park, Smart Materials and Structures 2016, 25; c) J. X. Li, S. Thamphiwatana, W. J. Liu, B. E. F. de Avila, P. Angsantikul, E. Sandraz, J. X. Wang, T. L. Xu, F. Soto, V. Ramez, X. L. Wang, W. W. Gao, L. F. Zhang, J. Wang, Acs Nano 2016, 10, 9536.
[15]   S. Tottori, L. Zhang, F. Qiu, K. K. Krawczyk, A. Franco-Obregon, B. J. Nelson, Adv Mater 2012, 24, 811.
[16]   B. Z. Cvetkovic, J. Puigmarti-Luis, D. Schaffhauser, T. Ryll, S. Schmid, P. S. Dittrich, Acs Nano 2012, 7, 183.
[17]   Y. Xia, G. M. Whitesides, Annual Review of Materials Science 1998, 28, 153.

A MOF-based microrobot that can be precisely navigated by weak rotational magnetic fields is presented. This soft-based microrobot is capable of performing single cell targeting in a cell culture media as well as a controlled delivery of cargo payloads in a regioselective manner inside a complex microfluidic channel network.

X. Wang, Dr. X. Chen, C. Alcântara, S. Sevim, Dr. M. Hoop, A. Terzopoulou, Dr. C. De Marco, Dr. C. Hu, Prof. A. J. DeMello, Prof. P. Falcaro, Prof. S. Furukawa, Prof. B. J. Nelson, Dr. J. Puigmartí-Luis,* and Dr. S. Pané

MOFBOTS: Metal–organic framework-based biomedical microrobots
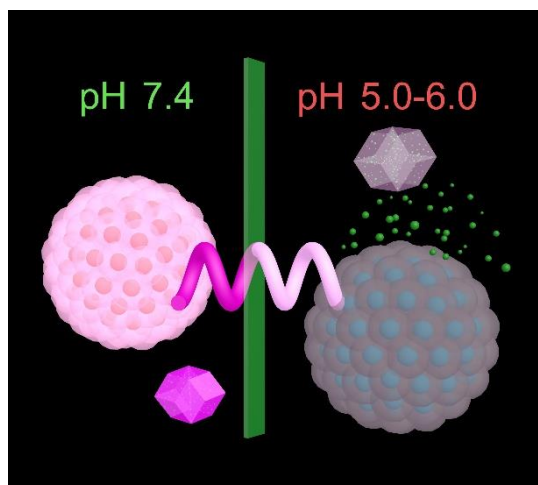
Supporting Information

MOFBOTS: Metal–organic framework-based biomedical microrobots

*Xiaopu Wang, Xiang-Zhong Chen, Carlos C.J. Alcântara, Semih Sevim, Marcus Hoop,
Anastasia Terzopoulou, Carmela de Marco, Chengzhi Hu, Andrew J. deMello, Paolo
Falcaro, Shuhei Furukawa, Bradley J. Nelson, Josep Puigmartí-Luis,* and Salvador Pané*

Synthesis of ZIF-8@ABFs with different reactant concentrations and reacting times

ZIF-8 coatings of varying thickness can be grown on the surface of an ABF by changing the
concentration of reactants and/or the reaction time. The compactness of ZIF-8 coatings can also
be tailored as a function of synthetic conditions, as shown in **Figure S1**a. We also found that
there is a specific range of concentrations in which ZIF-8 films can be formed. Within this range,
an increase in the concentration of reactants leads to an increase of the ZIF-8 crystal population
on the ABF. Figure S1b shows a photograph of solutions containing different concentrations of
reactants with a fixed concentration ratio (0.5) between $Zn(NO_3)_2$ and 2-methylimidazole. Note
that there is a certain concentration range within which ZIF-8 will grow. Below or over this
range (for our investigated case, 20mM - 400mM for $Zn(NO_3)_2$), ZIF-8 (solutions 1, and 8,9
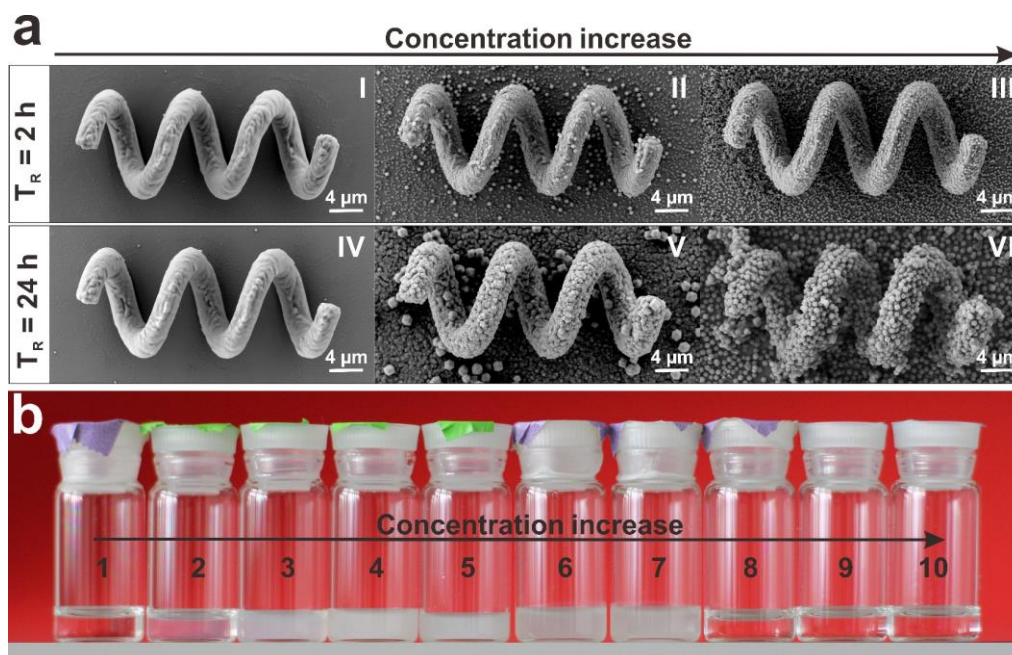and 10) will not form.

Figure S1. (a) SEM images of ZIF-8@ABFs. The ZIF-8 coatings in the upper row were obtained from a reaction time of 2 hours, with the concentration of $Zn(NO_3)_2$ increasing from left to right as follows: 10 mM (I); 25 mM (II); 50 mM (III); ZIF-8 coatings in the lower row were obtained from a 24 hour reaction time, with the concentration of $Zn(NO_3)_2$ increasing from left to right as follows: 10 mM (IV); 25 mM (V); 50 mM (VI). The ratio between $Zn(NO_3)_2$ and 2-methylimidazole concentrations was maintained at 0.5. (b) Formation of ZIF-8 at different reagent concentrations and with a fixed concentration ratio (0.5) between $Zn(NO_3)_2$ and 2-methylimidazole. The concentrations of $Zn(NO_3)_2$ (from 1 to 10) were 10 mM, 20 mM, 60 mM, 100 mM, 200 mM, 300 mM, 400 mM, 500 mM, 600 mM and 1000 mM, respectively.
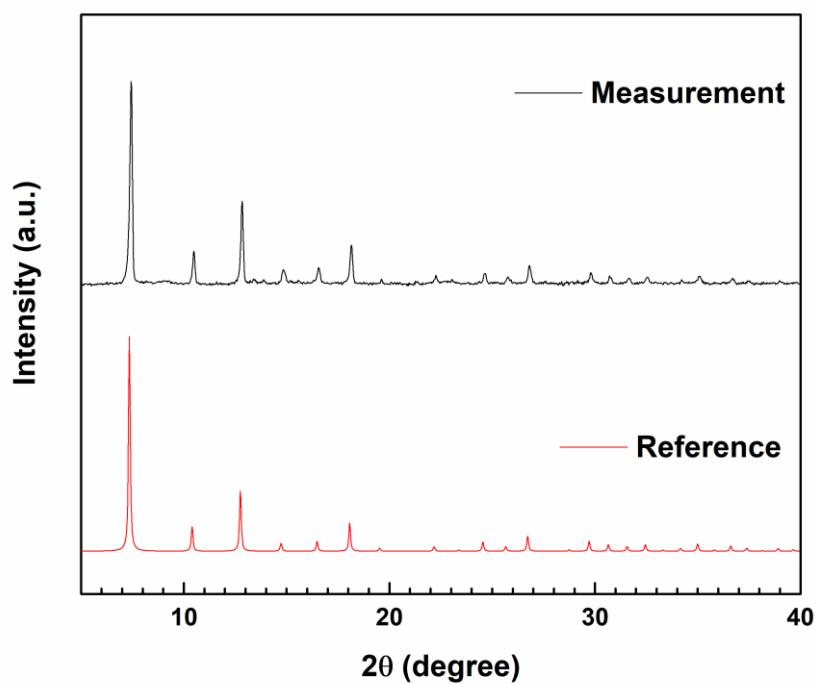
Figure S2. XRD pattern of ZIF-8 coating compared with the XRD pattern of ZIF-8 crystals in reference[13]